

Millisecond dips in the 2007-2009 RXTE/PCA lightcurve of Sco X-1 and one possible occultation event

Hsiang-Kuang Chang^{1,2*}, Chih-Yuan Liu², and Kuan-Ting Chen²

¹*Institute of Astronomy, National Tsing Hua University, Hsinchu 30013, Taiwan*

²*Department of Physics, National Tsing Hua University, Hsinchu 30013, Taiwan*

July 2010; September 2010

ABSTRACT

Serendipitous stellar occultation search is so far the only way to detect the existence of very small, very dim, remote objects in the solar system. To date, however, there are only very few reported detections for trans-Neptunian objects (TNOs) in optical bands. In the X-ray band, with the RXTE/PCA data of Sco X-1 taken from June 2007 to October 2009, we found one possible X-ray occultation event. We discuss the veracity and properties of this event, and suggest upper limits to the size distribution of TNOs at hectometer size and of Main-Belt Asteroids (MBAs) at decameter size.

Key words: occultations – Kuiper Belt – Solar system: formation – stars: neutron – X-rays: binaries.

1 INTRODUCTION

Population properties of small solar-system bodies, including main-belt asteroids (MBAs) and trans-Neptunian objects (TNOs), among others, carry information of the early solar system when planets were being formed and of the physics in the dynamical and collisional history of our solar system (see, for example, Kenyon et al. (2008); Bottke et al. (2005); O'Brien & Greenberg (2005); Cheng (2004)). Our knowledge of them, however, is far from being complete, particularly for those very small ones. Direct observation is so far achieved only for TNOs larger than deca-kilometers and for MBAs larger than about 400 meters. To pin down their size distribution at the small size end, searching for serendipitous stellar occultation events was proposed to be a possible way (Bailey 1976; Brown & Webster 1997; Roques & Moncuquet 2000; Cooray & Farmer 2003). Such search has been being conducted mainly in optical bands (Bianco et al. 2010; Bickerton, Kavelaars & Welch 2008; Roques et al. 2003) with few reported detections (Roques et al. 2006; Schlichting et al. 2009). In the X-ray band, in which occultation by even smaller objects may be more easily detected because of a smaller Fresnel scale, putative occultation events, allegedly caused by 100-meter size TNOs, were found in the 1996-2002 X-ray data of Sco X-1 taken by the instrument Proportional Counter Array (PCA) on board Rossi X-ray Timing Explorer (RXTE) (Chang et al. 2006, 2007). Those events, however, were later found to be most likely related to some instrumental dead-time effect of unknown na-

ture (Chang et al. 2007; Jones et al. 2008; Liu et al. 2008; Blocker, Protopapas & Alcock 2009). To get rid of instrumental effect contamination, new RXTE/PCA observations of Sco X-1 with a newly designed data mode to record detailed information of each PCA-detected high energy event have been being conducted since June 2007. It is hoped that those high energy events, which are called ‘very large events’ (VLEs) in RXTE/PCA terminology, can provide clear signature of possible instrumental effects.

In this paper we report the result we obtained from analyzing the new data taken from June 2007 to October 2009, which in total is about 240 ks. We found that VLEs, classified into different types according to the number of triggered anodes recorded in the data, can be used as an indicator of instrumental effects. In the 240-ks data, only 1 dip event is found to be unrelated to VLEs. We discuss the property of this dip event with occultation diffraction pattern fitting to its light curve. We then estimate upper limits to the size distribution of TNOs at hectometer size and of MBAs at decameter size, which are unattainable by any other means known to date.

2 DIP EVENTS AND THE RXTE/PCA VLES

The new RXTE observation of Sco X-1 started from June 13, 2007, and is still going on (RXTE ObsId 93067). Technical details of RXTE instrumentation can be found in the RXTE web site and also in Jahoda et al. (2006). To search for millisecond dip events, we adopted the same procedure employed in previous studies (Chang et al. 2006, 2007; Liu et al. 2008). We examined the light curves of Sco X-1

* E-mail: hkchang@phys.nthu.edu.tw

Type	number of triggered anodes	average count rate
A	no	1.73 ± 0.29
B	all	34.5 ± 11.2
C	more than one but not all	44.8 ± 9.80
D	only one	9.44 ± 2.27

Table 1. VLE types and their average count rates (in units of counts per second per PCU). The number of PCUs which are on during the observation varies from time to time. The total length of the data employed in this analysis is 240 ksec, and is 970 ksec-PCU when the number of PCU on is taken into account.

binned in different bin sizes from 1 ms to 10 ms. The deviation in photon counts of each bin in the light curve was determined by comparing its count number with the average counts and the count variance in an 8-s running window. In the 240-ks data that we use for this analysis, 39 ‘significant’ and 253 ‘less significant’ dips are found. To compare with our earlier works, we define ‘significant’ as those dips found in our searching algorithm with negative deviation larger than 6.5σ and ‘less significant’ as that between 5σ and 6.5σ . The choice of (minus) 6.5σ in previous works was to set a random probability at 0.001 for the analysis of the original 320-ks data employed in Chang et al. (2006), and (minus) 5σ is about the level below which the deviation distribution obviously shows excess compared to a normal distribution. We keep the same choice of the deviation level as in earlier works to have a better comparison. Readers are referred to Chang et al. (2006, 2007); Liu et al. (2008). for details of our searching algorithm. To investigate the connection between these dip events and possible instrumental effects, we examined detailed information of the recorded VLEs as described below.

RXTE/PCA VLEs are those events which deposit more than 100 keV in any one of the 6 active xenon anodes and the propane anode of one of the five identical proportional counter units (PCUs) of PCA. A VLE saturates the pre-amplifier and causes ringing in the signal chain when the amplified signal is restored to the baseline. Longer system dead time is set for VLEs, usually at $50\mu\text{s}$ for observations of Sco X-1. The actual duration in which the signal chains are affected depends on the pulse height of the saturating event. In default setting of RXTE/PCA observations, VLE count rates are recorded in a standard data mode with 125-ms time resolution. In the new observation of Sco X-1 (RXTE ObsID: 93067), to explore possible instrumental effects which may cause the millisecond dips in the PCA light curve of Sco X-1, a particular data mode was designed to retain detailed information of each individual VLE. In this data mode, the event epoch is recorded with $125\text{-}\mu\text{s}$ resolution and the identification of anodes triggered by the VLE is also recorded. With this new data mode, we found that some VLEs are very unusual in the way that no anode is recorded as having been triggered. We therefore classify VLEs into 4 types according to the number of triggered anodes as listed in Table 1, in which the averaged count rates (in units of counts per second per PCU) of these different VLEs are also listed. The count rate for all VLEs is 90.5 ± 19.2 counts per second per PCU. It is clear that Type-A VLEs are rare.

To study the association of the dip events that we found

Group	associated VLE type	significant dips	less significant dips
A	Type A	34	125
B	Type B, no Type A	2	94
C	Type C, no Type A, B	2	23
D	Type D only	0	3
E	no VLEs	1	8

Table 2. Number of dips in different groups.

with VLEs, we classify the dip events into 5 groups according to the type of VLEs that were detected within the time interval defined by the dip duration and one duration before the dip epoch. The number of dips in different groups is shown in Table 2. It is obvious that dip events are strongly related to Type-A VLEs. Among the 39 significant dips 34 are associated with Type-A VLEs, which are rare among all VLEs. It is not clear yet why a VLE is recorded in the data with no anode triggered. VLEs are usually caused by high energy particles. It may be possible that the incident particle is very energetic and an ionization avalanche or a secondary-particle shower is created so that the instrument suffers from a long sequence of dead time (Jones et al. 2008). For some unknown reasons all the VLE triggering flags are turned off. Although not yet fully understood, we conclude that Group-A dip events are instrumental.

To investigate whether dip events in other groups are also instrumental, we examine the consistency between the number of less significant dips and that due to random fluctuation. The deviation distribution of all the time bins in the light curve should be of a Poisson nature modified by the dead-time and coincidence-event effects if all the fluctuations are random and there is no occultation event. One example is shown in Figure 1 for a search with 2-ms time bins. Similar figures for earlier data can be found in Chang et al. (2006, 2007); Liu et al. (2008). From Figure 1 we can see that, although Gaussian distribution is a good approximation, the deviation distribution of the data is about a factor of $2 \sim 3$ lower than the Gaussian one at -5σ . In our current discussion we mainly consider the search with 2-ms bins since most of the less significant dips have a duration of 2 ms. If a Gaussian distribution is assumed, one expects to have 34.4 bins with photon counts less than 5σ below the average for 2-ms bins in the 240-ks data. Since some VLEs happen at the same time (within the $125\mu\text{s}$ time resolution) or within the same 2-ms bin, to estimate the distribution of these 34.4 bins in different dip groups, we first count the number of bins without any VLEs. The total amount of those bins is about 64.5 ks in the 120-ks data. Therefore, 18.5 of the 34.4 bins should be associated with Group E. For the other dip groups, we distribute the remaining 15.9 bins according to their related VLE count rates. The result is that, assuming a Gaussian distribution, there should be 0.3, 6.1, 7.9, 1.7, and 18.5 bins associated with Group A to E respectively. We note that this is in fact not strictly correct, because as mentioned above some VLEs happen in the same 2-ms time bin and we assign dip events into different groups with highest priority for Type-A VLEs, that is, there can be Type-B VLEs associated with Group-A dips.

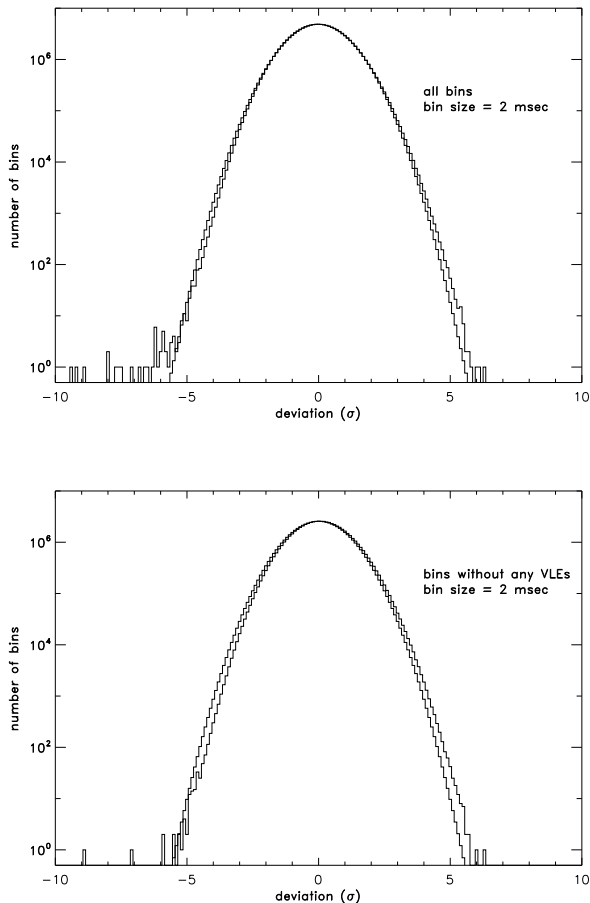


Figure 1. Deviation distribution of the Sco X-1 RXTE/PCA light curve based on the 240-ks data taken from June 2007 to October 2009 that we employed in this work. Thick histograms are from the data with 2-ms time bins, and thin histograms are the corresponding Gaussian distribution with the same total number of bins. The upper panel is for all the time bins, and the lower panel is for only those bins within which there are no VLEs. In the lower panel, most of those bins with large negative deviation, except for the one at about -7.1σ , are related to dip events of Group A-D, although within the 2-ms bin itself there is no VLE.

Nonetheless, the information here is enough for us to draw conclusions.

Comparing the numbers of less significant dips in different groups with those derived from a Gaussian distribution, and further taking into account the reduction by a factor of $2 \sim 3$, one can see that the numbers of less significant dips of Group A, B, C and D are not consistent with random fluctuation. There is a tendency that the excess of dip numbers decreases from Group A to Group D. Although details are not yet fully understood, it seems clear that Type-A VLEs are the most energetic and Type-D VLEs are the weakest. Because of the association with VLEs, all the Group A-D dips that are not due to random fluctuation are most likely instrumental. On the other hand, the number of less significant dips of Group E is roughly consistent with random fluctuation. We have no indication of instrumental effects for Group-E dips, which are not associated with any VLEs. The significant dip in Group E, which is found in the search with

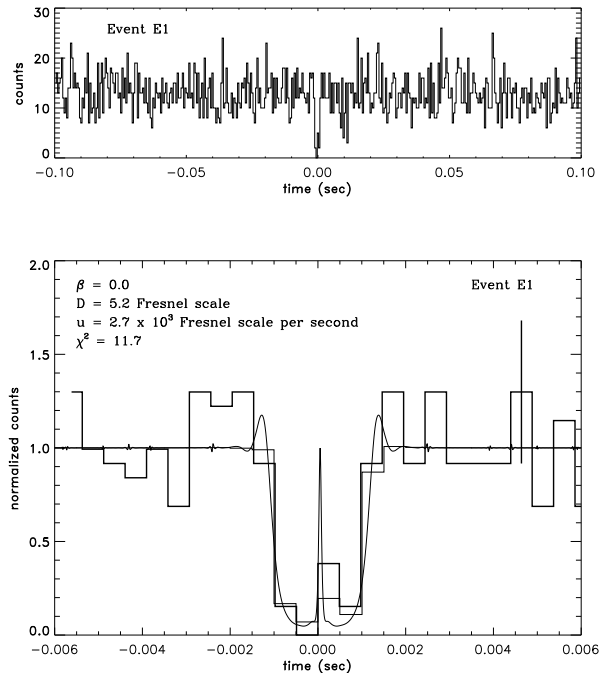


Figure 2. Light curves of Event E1. The upper panel shows the light curve 100-ms before and after Event E1 in 0.5-ms bins. The lower panel is a zoom-in view of Event E1. The thick histogram is the observed light curves in 0.5-ms bins, the thin curve is the computed diffraction pattern with best-fit parameters, and the thin histogram is the binned light curve of the computed one. The level of one- σ uncertainty in the observed light curve is indicated with a vertical bar. The average number of counts in a 0.5-ms bin is 13.1.

2-ms bins, has a deviation of -7.1σ , corresponding to a random probability of less than 7.5×10^{-5} in the 240-ks data. We denote this dip event as Event E1, whose light curve is plotted in Figure 2, together with the best-fit diffraction pattern described in the next section.

3 DISTANCE AND SIZE OF THE OCCULTING BODIES

Event E1, a non-instrumental millisecond dip event, is most likely an occultation event caused by objects in the solar system (Chang et al. 2006, 2007). The observed light curve, indeed, can be well described by shadows of occultation when diffraction is properly taken into account. In the following we explain how we conduct the diffraction pattern fitting and how we estimate the distance and size of the occulting body with fitting results and assumed orbital parameters.

3.1 Fitting the occultation light curve with diffraction patterns

In our study we assume the occulting body is a spherical one and the background star, Sco X-1, is a distant point source. We also take into account the actual RXTE/PCA observed Sco X-1 spectrum, which peaks at 4 keV. We note that the shadow diffraction patterns are all the same for a given ratio

of the occulting body diameter to the Fresnel scale when the length is expressed in units of the Fresnel scale. Hereafter we denote that ratio with α . To describe an occultation light curve, 4 more parameters are needed. One is the impact parameter β , which is defined as the closest distance of the crossing path to the shadow center in units of the occulting body radius. Another one is the transverse relative speed u_t of the observer with respect to the shadow. The third is the epoch of the central crossing, t_0 , and the fourth is the normalization N . For each occultation light curve, to find a best fit in the 5-parameter space $(\alpha, \beta, u_t, t_0, N)$ is not practical. We therefore search for the ‘best’ fit in the following way. We fix β at certain different values, e.g., from 0 to 1 with an increment step of 0.1. For a fixed β , we compute theoretical occultation light curves over a range of α . For each computed light curve of a given α, u_t over a certain range is applied to convert the length of the computed pattern into time and the computed curve is folded into a binned curve to compare with data.

In this study, we use data curves with 0.5-ms bins. The normalization N of the computed curve is set to be the average counts per bin of the data curve in the fitting window, which we choose to be 12.5 ms, that is, 25 bins. With given β, α, u_t , and N , we adjust t_0 with a step size of 0.05 ms, which is 0.1 time bin, to look for the smallest χ^2 between the binned curve and data curve. We then assign this χ^2 to be the fitting result of this set of parameters β, α , and u_t . The ‘best’ fit is determined by the minimum χ^2 in the parameter space of β, α , and u_t as described above.

The best fit result for Event E1 is that $\chi^2 = 11.7$ (with 20 degrees of freedom), $\beta = 0.0$, $\alpha = 5.2_{-2.6}$ and $u_t = 2700_{-1450}$ Fresnel scale per second. The uncertainty quoted above is at the 3- σ level in the α - u_t space for a fixed β . Here we report only the lower uncertainty level, since a combination of large u_t and large α gives acceptable fits; see Figure 3. The reason is that the light curve of Event E1 does not show clear side lobes. Diffraction patterns of large u_t and α therefore cannot be discriminated. Those patterns correspond to occultation caused by very nearby objects (see the next subsection). The uncertainty in α quoted here is the value corresponding to the uncertainty in u_t , rather than the α extreme values on the 3- σ level contour. It is because that our interest in α is for estimating the diameter of the occulting body, which depends on both u_t and α in a non-trivial way, and the distance estimate depends on u_t only. The β dependence of the diffraction pattern fitting is weak. The best-fit χ^2 value (11.7 for 20 d.o.f.) is very low. It only shows that the light curve can be described by a diffraction pattern, but at the same time provides less power in discriminating fitting parameters. This low χ^2 value are due the following two factors. One is the low count number in each bin, which gives a relatively large error bar, and the other is the 0.5-ms bin size, which is large so that details of a diffraction pattern are smeared out. These two factors make it easy to obtain a low χ^2 value fitting.

3.2 Distance and size determination assuming a circular orbit

Based on the best estimated value of the relative transverse speed between RXTE and the shadow obtained from diffraction pattern fitting and the knowledge of RXTE’s velocity

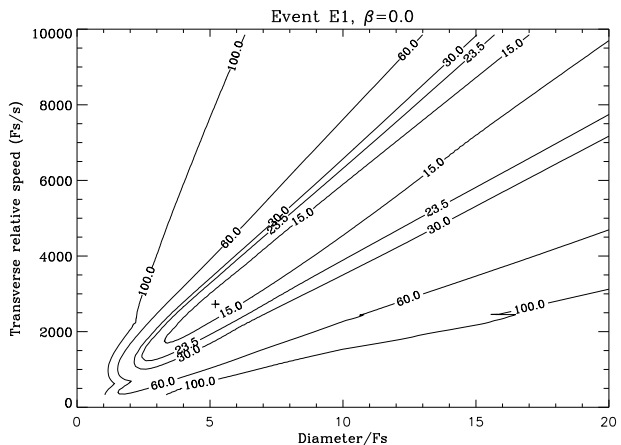


Figure 3. χ^2 contours of the diffraction pattern fitting in the α - u_t parameter space for Event E1. The cross symbol marks the location where the smallest χ^2 value is found.

at the event epoch (given in Table 3), one may infer the distance to the occulting body by assuming its orbital parameters. This assumption is needed because of the size-distance degeneracy, as one can see that u_t can be determined from diffraction pattern fitting only in units of Fresnel scale per second and the Fresnel scale is distance dependent. Since most of MBAs and TNOs have low-eccentricity orbits, for simplicity and as an approximation, we consider only circular orbits in this study, but allow different orbital inclination. In Figure 4, the relative speed transverse to the Sco X-1 direction between RXTE and the occulting body as a function of heliocentric distance of the occulting body is plotted, and so is the relative speed determined from diffraction pattern fitting, which is translated from the form of Fresnel scale per second into real speed as a function of heliocentric distance of the occulting body. The intersection of these two curves gives the estimate of the heliocentric distance of the occulting body. From that distance, one may infer the diameter of the occulting body from the best estimated value of the diameter to Fresnel scale ratio α , also obtained from the diffraction pattern fitting.

From Figure 4, considering the curve for the minimum inclination (the thick solid line in Figure 4), we obtain that the heliocentric distance and diameter of the occulting body are $r = 3.4_{-2.4}^{+24}$ AU and $D = 38_{-37}^{+26}$ m. The uncertainty quoted here is based on the uncertainty of the diffraction pattern fitting. Because the fitting does not provide constraint for high u_t , we do not have corresponding constraint at the small distance end in Figure 4. In fact, a very nearby object of meter size and with speed at a few kilometers per second could produce a light curve like Event E1. This corresponds to high u_t and high α because of the very small Fresnel scale at a very nearby distance. We therefore artificially assign the lower uncertainty level to r and D in such a way to symbolically indicate such a situation. On the other hand, the curve for the largest relative speed (the thick dashed line) in Figure 4 at about 40 AU corresponds to an inclination angle of 172° (retrograde orbits). If we consider high-inclination orbits, within the 3- σ fitting uncertainty, the occulting body could be at about 40 AU (and therefor about 150 m in size). Of course, such orbits are rare.

Epoch	RXTE location (km)	RXTE velocity (km/s)
MJD 54622.397997210 (2008-06-05)	$X = -3.947533 \times 10^7$ $Y = -1.338443 \times 10^8$ $Z = -5.803026 \times 10^7$	$V_X = +3.482881 \times 10^1$ $V_Y = -1.043335 \times 10^1$ $V_Z = -9.082142 \times 10^{-1}$

Table 3. Spacecraft information for Event E1. The RXTE location and velocity at the event epoch are expressed in the celestial equatorial coordinate system. The X-axis is in the direction of the vernal equinox, the Z-axis is in the north celestial pole direction, and the solar system barycenter is at the origin. These values are obtained from RXTE housekeeping data and the ephemeris of the Earth (JPL Horizons On-Line Ephemeris System, <http://ssd.jpl.nasa.gov/horizons.html>). The direction of Sco X-1 is R.A. = $16^h 19^m 55.07^s$, Dec. = $-15^\circ 38' 25.0''$ and its solar elongation at the event epoch is 169.3° .

Because of the size-distance degeneracy and the weak constraints that diffraction pattern fitting to the Event-E1 light curve can provide, we are not able to draw firm conclusions on the distance and size of the occulting body causing Event E1. The size-distance degeneracy may be resolved by the knowledge of the occulting-body orbit, which is usually not available and needs to be assumed, or by an array of detectors, which, although not yet available now, may provide information of the shadow size directly. In the following sections we discuss what constraints we may have on the MBA and TNO size distributions based on the search over the 240-ks RXTE/PCA data of Sco X-1. The result is plotted in Figure 5. We note that, limited by the RXTE/PCA count rate of Sco X-1, which is about 2×10^4 counts per second per PCU, our dip-event search algorithm can detect occultation events caused by objects of size only down to one or two times Fresnel scale (Chang et al. 2007).

4 THE MBA SIZE DISTRIBUTION

Direct observation of the main belt asteroids has only been achieved down to the size of about 400 meters. Earlier surveys revealed a wavy size distribution of MBAs with a bump around 100 km and a second one around 5 km (see Fig. 4 in Cheng (2004) and Fig. 14 in O'Brien & Greenberg (2005) for a compiled distribution; see also Tedesco & Desert (2002) for the ISO result, Ivezić et al. (2001) for SDSS, and Yoshida & Makamura (2007) for Subaru survey). It appears that most of the results are consistent with a power index of -3 (5 - 40 km) and of -1.3 (0.4 - 5 km) for the cumulative distribution. An estimate of the cumulative number of MBAs, based on the ISO result, is $(1.2 \pm 0.5) \times 10^6$ for MBAs with diameter larger than 1 km.

To estimate the occultation event rate, we formulate the MBA size distribution as the following:

$$N_{>D} = N_i \left(\frac{D}{D_i} \right)^{-b_i}, \quad (1)$$

with $D_1 = 5$ km, $b_1 = 3$, $N_1 = 1.5 \times 10^5$ for 5 km $< D < 40$ km, $D_2 = 1$ km, $b_2 = 1.3$, $N_2 = 1.2 \times 10^6$ for 0.4 km $< D < 5$ km, and $D_3 = 0.4$ km, $b_3 = 2.5$, $N_3 = 3.9 \times 10^6$ for $D < 0.4$ km. In this formulation, the normalization is set according to the ISO result, and the power index 2.5 for the state of collisional equilibrium with a constant tensile strength is assumed for $D < 0.4$ km. The expected event rate can be estimated as

$$R_e = \frac{1}{\tau} \frac{\Omega_\tau}{\Omega_A}, \quad (2)$$

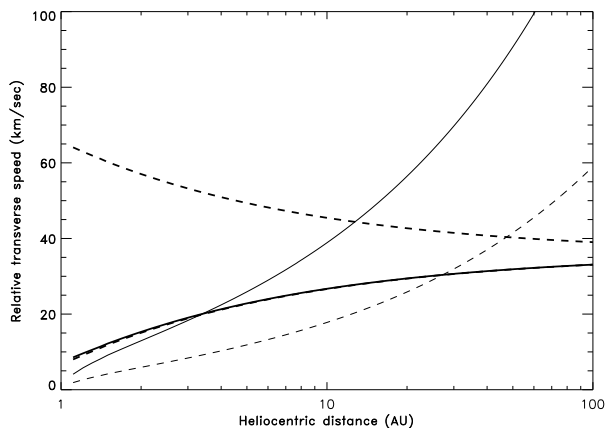


Figure 4. Estimate of the occulting body distance for Event E1. The thick curves are the relative speed transverse to the Sco X-1 direction between RXTE and the occulting body, whose orbit is assumed to be a circular one. The thick solid curve is for the case of a minimum orbital inclination. The thick dashed curves give the largest and smallest relative transverse speed when all the possible orbital inclination is considered. The lower thick dashed curve almost coincident with the thick solid one. In this computation, RXTE velocity in the solar system at the event epoch and the Sco X-1 direction, which is 5.5 degrees north of the ecliptic, are both taken into account. The thin curves are the relative transverse speed determined from diffraction pattern fitting. The thin solid one is the best fit and the thin dashed one give the uncertainty at the $3\text{-}\sigma$ level. For Event E1, diffraction pattern fitting does not provide good constraint to the higher end of the relative speed, because of lacking of side lobes.

where Ω_τ is the sky area swept by all MBAs in the time interval of τ , and Ω_A is the sky area over which MBAs are distributed. We then have, for MBAs with diameter larger than 10 m,

$$\Omega_\tau = \int_{10\text{m}}^{\infty} \frac{1}{\Delta^2} \frac{dN}{dD} D v \tau dD \quad (3)$$

$$= \left\langle \frac{v}{\Delta^2} \right\rangle \tau \times 6.6 \times 10^8 \text{ km}, \quad (4)$$

where typical values of v , the relative speed, and Δ , the distance from the earth to the MBA, need to be assumed, and about 99.3% contribution comes from those with diameter smaller than 0.4 km. Adopting $\Delta = 2$ AU and $v = 12.6$ km/s, we have

$$\Omega_\tau = 3.7 \times 10^{-8} \tau \text{ s}^{-1}. \quad (5)$$

The ecliptic latitude distribution of about 13,000 MBAs

with $r^* < 21.5$ is shown in Fig. 12 of Ivezić et al. (2001). Considering that Sco X-1 is at 5.5° north of the ecliptic, we adopt an equivalent sky coverage area as being spanning over 20° around the ecliptic, that is,

$$\Omega_A \approx 360 \times 20 \times \left(\frac{\pi}{180}\right)^2 \approx 2.2. \quad (6)$$

The expected event rate, R_e is therefore about $1.7 \times 10^{-8} \text{ s}^{-1}$.

If we consider that Event E1 is caused by an MBA, the measured event rate with one detection (Event E1) is $R_m = (1/240 \text{ ks}) \approx 4.2 \times 10^{-6} \text{ s}^{-1}$. R_m is about 250 times larger than R_e . However, if that is the case, the MBA causing Event E1 is about 40 m in size. The chance is low that one 40-m object is found but no smaller ones, unless the number of MBAs drops significantly for size smaller than 40 m. If so and still assuming a single power law for size smaller than 400 m, to have one detection in 240 ks for MBAs down to 40 m in size, the power index b_3 will need to be 5.8. It is a very steep power law, as shown in Figure 5, and also requires the paucity of smaller MBAs. We consider this possibility not plausible.

If Event E1 is not caused by an MBA, we have no detection of MBAs in the 240-ks data. Our dip-event search algorithm can detect occultation events caused by objects of size only down to one or two times Fresnel scale (Chang et al. 2007). For the MBA distance, it is about 10 m. Based on the non-detection, we estimate the upper limit to the size distribution at the level of assuming one detection. As calculated above, this level will give a detection rate 250 times larger than R_e . To have such a detection rate, if we still adopt a single power law for the size range between 10 m and 400 m, the power index b_3 needs to be 4.0, instead of 2.5. This is quite steep, although a power index larger than 2.5 is usually expected. In the collisional equilibrium, one expects to have (O'Brien & Greenberg 2003)

$$b_3 + 1 = \frac{7 + s/3}{2 + s/3}, \quad (7)$$

where s is the power index of the strength-size relation. For $b_3 = 4.0$, we have $s = -2.25$, which is larger than all the results reported in the literature to date.

5 THE TNO SIZE DISTRIBUTION

We describe the TNO size distribution in terms of the differential surface density at ecliptic. More specifically, we plot in this paper the quantity $\frac{dn}{d \log s}$ versus s , where dn is the differential number of TNOs **per square degree** of size between s and $s + ds$ and s is the diameter.

5.1 RXTE observations

For a background point source, the event rate is

$$\frac{N}{T} = \frac{\int_{s_1}^{s_2} \left(\frac{dn}{ds}\right) sv ds}{d^2} \times \left(\frac{180}{\pi}\right)^2, \quad (8)$$

where N is the number of detected events (assuming a 100% detection efficiency), T the total exposure time, $\left(\frac{dn}{ds}\right)$ the differential size distribution (in terms of surface density), v

the typical sky-projection relative speed, and d the typical distance to the TNOs.

To derive $\left(\frac{dn}{ds}\right)$ from the event rate, a functional form of the distribution needs to be assumed. On the other hand, if the integration is only over a small range of the size, we may derive an average value at that size. Noting that $\frac{dn}{d \log s} = \frac{dn}{ds} s \ln 10$, we have

$$\int_{s_1}^{s_2} \left(\frac{dn}{ds}\right) sv ds = \left(\frac{dn}{d \log s}\right)_{s_1 < s < s_2} \frac{v(s_2 - s_1)}{\ln 10}, \quad (9)$$

and

$$\left(\frac{dn}{d \log s}\right)_{s_1 < s < s_2} = \frac{d^2}{v(s_2 - s_1)} \frac{N}{T} \ln 10 \left(\frac{\pi}{180}\right)^2. \quad (10)$$

Assuming a typical distance $d = 43 \text{ AU}$ and a typical relative sky-projection speed $v = 30 \text{ km/s}$, with $T = 240 \text{ ks}$ and setting one detection as the upper limit, we have in the size range from 60 m to 300 m

$$\left(\frac{dn}{d \log s}\right) < 1.7 \times 10^{10} \text{ deg}^{-2}. \quad (11)$$

The ecliptic latitude distribution of TNOs is not yet well determined. To be more precise, one should discuss the latitude with respect to the Kuiper Belt Plane (KBP) (Elliot et al. 2005) rather than to the ecliptic, but the difference is not large. Sco X-1 is 5.5° north of the ecliptic and 4.9° north of the KBP. The CFHT survey (Trujillo, Jewitt & Luu 2001) reported a 20° half-angle of an assumed gaussian distribution in orbital inclination (with respect to the ecliptic). This half-angle in the inclination distribution translates to about 12.8° for a corresponding half-angle in the apparent ecliptic latitude distribution, assuming circular orbits. With this distribution, a factor of 1.14 should be applied to convert the estimate at the Sco X-1 latitude to the ecliptic. However, if we adopt the distribution reported in Elliot et al. (2005), a factor of 4 should be applied for conversion to the KBP. In this paper we use the latitude distribution of Trujillo, Jewitt & Luu (2001).

5.2 TNOs larger than 100 km

For large TNOs, we use a recent result reported in Fuentes, George & Holman (2009), in which a double-power-law model describes well the luminosity function down to R -band magnitude of about 27. With the notation employed in that paper, the differential luminosity function reads

$$\sigma(R) = C(10^{-\alpha_1(R-23)} + 10^{(\alpha_2 - \alpha_1)(R_{\text{eq}} - 23)} 10^{-\alpha_2(R-23)})^{-1} \quad (12)$$

and

$$C = \sigma_{23}(1 + 10^{(\alpha_2 - \alpha_1)(R_{\text{eq}} - 23)}), \quad (13)$$

where $\sigma(R)$ is, with our notation here, equal to $-\frac{dn}{dR}$. The reported best fit values of the parameters in that distribution are $\alpha_1 = 0.73_{-0.09}^{+0.08}$, $\alpha_2 = 0.20_{-0.14}^{+0.12}$, $R_{\text{eq}} = 25.0_{-0.6}^{+0.8}$, and $\sigma_{23} = 1.46_{-0.12}^{+0.14}$. C is therefore equal to 1.59. To convert the luminosity function into the size distribution, we assume a constant albedo and the same distance for all TNOs, and note that

$$s = 10^{-\left(\frac{R - R_{\text{eq}}}{5}\right)} s_{\text{eq}}. \quad (14)$$

It follows that

$$\begin{aligned} \frac{dn}{ds} &= \sigma(R) \frac{5}{\ln 10} \frac{1}{s_{\text{eq}}} 10^{\frac{R-R_{\text{eq}}}{5}} \\ &= \frac{5}{\ln 10} \frac{C}{s} 10^{\alpha_1(R_{\text{eq}}-23)} \left[\left(\frac{s}{s_{\text{eq}}} \right)^{5\alpha_1} + \left(\frac{s}{s_{\text{eq}}} \right)^{5\alpha_2} \right]^{-1} \end{aligned} \quad (15)$$

and

$$\begin{aligned} \frac{dn}{d \log s} &= \frac{dn}{ds} s \ln 10 \\ &= 5C 10^{\alpha_1(R_{\text{eq}}-23)} \left[\left(\frac{s}{s_{\text{eq}}} \right)^{5\alpha_1} + \left(\frac{s}{s_{\text{eq}}} \right)^{5\alpha_2} \right]^{-1} \end{aligned} \quad (16)$$

Adopting $s_{\text{eq}} = 90$ km at $R_{\text{eq}} = 25$, which assumes an albedo of 4% and a distance of 42 AU and adopts $m_R = -27.6$ for the R -band magnitude of the Sun (Fuentes, George & Holman (2009), see also Fraser & Kavelaars (2009)), we have, at $s = 90$ km, that

$$\frac{dn}{d \log s} = 1.1 \times 10^2 \text{ deg}^{-2}. \quad (17)$$

5.3 TNOs of size at 500 m (observations of HST/FGS)

Schlichting et al. (2009) reported the detection of an occultation event by a TNO of 500 m diameter in the HST/FGS archival data. They suggest a power index $q = 3.9 \pm 0.03$ for the TNO differential size distribution below 90 km and the accumulated number of TNOs larger than 500 m is $2.1_{-1.7}^{+4.8} \times 10^7 \text{ deg}^{-2}$. These values can be converted into $\left(\frac{dn}{d \log s}\right)$ in the following way. The accumulated distribution is

$$\Sigma_{>s} = C_1 \left(\frac{s}{s_0} \right)^{1-q}, \quad (18)$$

and

$$\begin{aligned} \frac{dn}{d \log s} &= \frac{dn}{ds} s \ln 10 \\ &= (1-q) C_1 \left(\frac{s}{s_0} \right)^{-q} \frac{s}{s_0} \ln 10. \end{aligned} \quad (19)$$

For $s_0 = 500$ m, $C_1 = 2.1_{-1.7}^{+4.8} \times 10^7 \text{ deg}^{-2}$. We therefore have at $s = 500$ m that

$$\frac{dn}{d \log s} = 1.4_{-1.1}^{+3.2} \times 10^8 \text{ deg}^{-2}. \quad (20)$$

6 SUMMARY AND DISCUSSION

In the 240-ks RXTE/PCA data of Sco X-1 taken from June 2007 to October 2009, we found that millisecond dip events in the light curve are related to VLEs, which in turn suggests an instrumental origin for those millisecond dips. The relation is strongest for Type-A VLEs and weakest for Type D. One dip event (denoted as Event E1 in this paper) at random probability of less than 7.5×10^{-5} is found to be unrelated to any VLEs. The slight asymmetry, which is similar to many of the VLE-related dips, and the lacking of side lobes in the light curve of Event E1 cast some doubts on its nature being an occultation event. However, since the count number

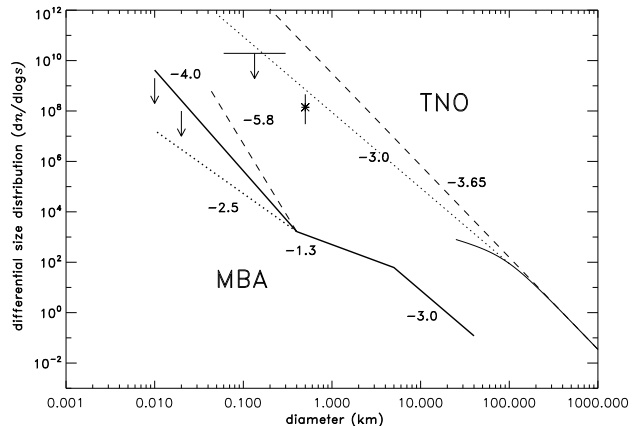


Figure 5. Size distributions of main-belt asteroids (MBAs) and trans-Neptunian objects (TNOs). Plotted here is the differential sky surface density at the ecliptic per decade of size in units of number per square degree. For TNOs, the upper limit at about 0.1 km, denoted with a downward arrow, is derived from our non-detection in the 240-ks RXTE/PCA data of Sco X-1, and is set at the level of one detection in 240 ks. The asterisk symbol at 0.5 km is based on the reported HST/FGS detection of an occultation event (Schlichting et al. 2009). The thin solid curve is the double-power-law distribution of large TNOs (Fuentes, George & Holman 2009), which shows a break at 90 km. The HST/FGS result supports the existence of such a break, so does our current result. The thin dashed line is a direct extrapolation from the large size end of the double-power-law towards smaller size and the thin dotted line is a power law anchoring on the double-power-law at 90 km with a power index of -3.0. We note that all the power indices in this figure, explicitly printed close to the corresponding power-law lines, are for the differential size distribution per decade of size, and are therefore the same as that of the cumulative size distribution. Upper limits derived from other observations are all above the thin dashed line and can be found in Schlichting et al. (2009). The double-power-law and the HST/FGS result in fact indicate a wavy shape for the TNO size distribution, which is similar to the behaviour of MBAs, plotted in the lower left half in this figure. The thick lines with power indices -1.3 and -3.0 are for MBAs larger than 0.4 km, which are directly observable. The MBA size distribution has a wavy shape with two bumps at about 100 km (not shown in this figure) and 5 km. The thick dotted line with a power index of -2.5 is for a size distribution in collisional equilibrium assuming a constant structure strength of MBAs in that size range. The thick dashed line with a power index of -5.8 is the one implied by Event E1 being caused by a 40-m MBA. The thick solid line with a power index of -4.0 is the upper limit at the level of assuming one detection down to 10 meters.

is small (the central 4 bins in the light curve plotted in Figure 2 have 2, 0, 5, and 2 counts respectively), one probably should treat the light curve with high uncertainty. It is also because of the low count number, diffraction pattern fitting does not provide strong enough information to constrain the property of the occulting body if it is indeed an occultation event, although acceptable fittings can be easily obtained. As discussed in previous sections, it might be due to a TNO of 150-m size, but with a rare retrograde orbit, or, it might be due to an MBA of 40-m size, but the associated detection rate is incredibly high, or, it might be due to a very nearby object of meter size moving at a relative speed of a

few kilometers per second. Given all these uncertainties, we proceed to estimate the upper limits to the size distribution of TNOs and MBAs at the level of assuming one detection.

The TNO size distribution has been studied in several previous works, e.g., Bianco et al. (2010); Schlichting et al. (2009); Fraser & Kavelaars (2009); Fuentes, George & Holman (2009); Bickerton, Kavelaars & Welch (2008); Liu et al. (2008); Roques et al. (2006); Bernstein et al. (2004). In this paper we provide the most updated upper limit at the hectometer size, which is a size range that optical occultation surveys are unable to explore. Readers are referred to the caption of Figure 5 for more discussion.

The MBA size distribution has been studied by several surveys (Ivezic et al. 2001; Tedesco & Desert 2002; Yoshida & Makamura 2007) down to the size of 400 meters. For smaller ones, if the collisional equilibrium and a constant tensile strength are assumed, a power law with power index -2.5 (cumulative) is expected (Dohnanyi 1969; O'Brien & Greenberg 2003). However, the tensile strength is known to be size dependent, and the size distribution for the size range in the so-called strength-scaled regime in collisional equilibrium is expected to be steeper than the constant-strength solution (Benz & Asphaug 1999; O'Brien & Greenberg 2003). The upper limit that we estimate, as shown in Figure 5, has a power index -4.0 , which in turn suggests a power index of -2.25 for the strength-size relation (O'Brien & Greenberg 2003), expressed in the form of the critical specific energy (conventionally denoted with Q_D^*) as a function of size. This is still much steeper than all the reported strength-size relation in the literature to our knowledge, of which the steepest one has a power index of about -1 (Durda, Greenberg & Jedicke 1998).

Studying population properties of small TNOs and MBAs with serendipitous occultation events in X-rays is still in its infant stage, currently only possible for RXTE/PCA, the X-ray instrument with the largest effective area, observing Sco X-1, the brightest X-ray source in the sky. It, however, suffers significantly from the instrumental dead time caused by high energy events. Observations with RXTE and future facilities, such as ASTROSAT/LAXPC, AXTAR (Chakrabarty et al. 2008), and IXO, together with a more rigorous design of the survey, similar to those considered in the optical band (Bickerton, Welch & Kavelaars 2009; Nihei et al. 2007; Gaudi 2004), will be able to yield more reliable and complete information, particularly when more X-ray sources in different directions can be employed.

ACKNOWLEDGMENTS

We thank Ed Morgan, who designed the new RXTE/PCA data mode and coordinated the new RXTE observations of Sco X-1, and Jau-Shian Liang, who helped to identify RXTE velocity in the solar system at the event epochs. We appreciate very much Steve Bickerton's comments, which significantly improved this paper. We are also grateful to Françoise Roques, Alain Doressoundiram, and Sun-Kung King for helpful discussion. This work was supported by the National Science Council of the Republic of China under grant NSC 96-2628-M-007-012-MY3.

REFERENCES

- Bailey M.E., 1976, *Nature*, 259, 290
 Benz W., Asphaug E., 1999, *Icarus*, 142, 5
 Bernstein G.M., Trilling D.E., Allen R.L., Brown M.E., Holman M., Malhotra R., 2004, *AJ*, 128, 1364
 Bianco F.B. et al., 2010, *AJ*, 139, 1499
 Bickerton S.J., Kavelaars J.J., Welch D.L., 2008, *AJ*, 135, 1039
 Bickerton S.J., Welch D.L., Kavelaars J.J., 2009, *AJ*, 137, 4270
 Blocker A.W., Protopapas P., Alcock C.R., 2009, *ApJ*, 701, 1742
 Bottke W.F., Durda D.D., Nesvorný D., Jedicke R., Morbidelli A., Vokrouhlický D., Levison H.F., 2005, *Icarus*, 179, 63
 Brown M.J.I., Webster R.L., 1997, *MNRAS*, 289, 783
 Chang H.-K., King S.-K., Liang J.-S., Wu P.-S., Lin L.C.-C., Chiu J.-L., 2006, *Nature*, 442, 660
 Chang H.-K., Liang J.-S., Liu C.-Y., King S.-K., 2007, *MNRAS*, 378, 1287
 Chakrabarty D., Ray P.S., Strohmayer T.E., the AXTAR Collaboration, 2008, *AIP Conf. Proc.* 1068, 227
 Cheng A.F., 2004, *Icarus*, 169, 357
 Cooray A., Farmer A.J., 2003, *ApJ*, 587, L125
 Dohnanyi J.W., 1969, *JGR*, 74, 2531
 Durda D.D., Greenberg R., Jedicke R., 1998, *Icarus*, 135, 431
 Elliot J.L. et al., 2005, *AJ*, 129, 1117
 Fraser W.C., Kavelaars J.J., 2009, *AJ*, 137, 72
 Fuentes C.I., George M.R., Holman M.J., 2009, *ApJ*, 696, 91
 Gaudi B.S., 2004, *ApJ*, 610, 1199
 Ivezic, Z. et al., 2001, *AJ*, 122, 2749
 Jahoda K. et al., 2006, *ApJS*, 163, 401
 Jones T.A., Levine A.M., Morgan E.H., Rappaport S., 2008, *ApJ*, 677, 1241
 Kenyon S.J., Bromley B.C., O'Brien D.P., Davis D.R., 2008, in *The Solar System Beyond Neptune*, M.A. Barucci, H. Boehnhardt, D.P. Cruikshank, and A. Morbidelli (eds.), University of Arizona Press, Tucson, page 293-313
 Liu C.-Y., Chang H.-K., Liang J.-S., King S.-K., 2008, *MNRAS*, 388, L44
 Nihei T.C., Lehner M.J., Bianco F.B., King S.-K., Giannamarco J.M., Alcock C., 2007, *AJ*, 134, 1596
 O'Brien D.P., Greenberg R., 2003, *Icarus*, 164, 334
 O'Brien D.P., Greenberg R., 2005, *Icarus*, 178, 434
 Roques F. et al., 2006, *AJ*, 132, 819
 Roques F., Moncuquet M., 2000, *Icarus*, 147, 530
 Roques F., Moncuquet M., Lavilloniere N., Auvergne M., Chevreton M., Colas F., Lecacheux J., 2003, *ApJ*, 594, L63
 Roques F., Moncuquet M., Sicardy B., 1987, *AJ*, 93, 1549
 Schlichting H.E., Ofek E.O., Wenz M., Sari R., Gal-Yam A., Livio M., Nelan E., Zucker S., 2009, *Nature*, 462, 895
 Tedesco E., Desert F.-X., 2002, *AJ*, 123, 2070
 Trujillo C.A., Jewitt D.C., Luu J.X., 2001, *AJ*, 122, 457
 Yoshida F., Nakamura T., 2007, *P&SS*, 55, 1113